LoRaWAN Underground to Aboveground Data Transmission Performances for Different Soil Compositions

Gabriele Di Renzone, Stefano Parrino, Giacomo Peruzzi, Alessandro Pozzebon, *Member, IEEE*, and Duccio Bertoni

***Abstract*— The aim of this article is to discuss the usability of the long-range (LoRa) transmission technology together with the LoRa wide-area network (LoRaWAN) protocol for underground monitoring activities. In particular, this article focuses on the transmission performances in different soils (i.e., gravel, sand, and clay), for an underground-to-aboveground (UG2AG) communication. The three soils have been chosen in order to test the system behavior in case of pure soil compositions, in order to provide a general result that can be used to evaluate the transmission chances for any kind of soil. The performances of the transmission channel have been tested using an experimental setup for depths up to 50 cm, acquiring the values of the received signal strength indicator (RSSI) and the signal-to-noise ratio (SNR) for every transmission and analyzing the packet loss (PL). Such a kind of system may be crucial in several application scenarios, such as environmental monitoring or smart agriculture, where the real-time, remote acquisition of underground parameters at different depths is required.**

***Index Terms*— Internet of Things (IoT), long-range wide-area network (LoRaWAN), performance analysis, soil composition, underground-to-aboveground (UG2AG) transmission.**

I. Introduction

WIRELESS underground sensor networks (WUSNs) have been increasingly investigated since the need of establishing pervasive monitoring infrastructures to be deployed in unreachable and hostile environments has become more and more compelling over time [1]–[3]. Moreover, the design phases of such networks are notably more challenging than for the superficially deployed ones due to the intrinsic attenuation properties of soil. Despite it, the growing necessity of WUSN gradually coined the brand new paradigm of the Internet of Underground Things (IoUT) [4], which is currently paving the way for novel solutions for measuring, sampling, and transmitting the extent of various phenomena that take place underground, whose knowledge is required in order to actuate the most diverse operations either aboveground or underground (e.g., manage assets, predict occurrence of events, perform maintenance, schedule processes, and so on). To this end, several techniques for underground-to-underground (UG2UG), underground-to-aboveground (UG2AG), and aboveground-to-underground (AG2UG) transmissions have been devised in disparate contexts: oil and gas reservoirs [5], smart lighting systems [6], smart urban drainage systems [7], smart cities [8], and environmental monitoring [9] are only few instances although smart agriculture has taking a huge advantage from such technologies [10]–[15].

In this article, an IoUT sensor node, which is suitable to any of the aforementioned scenarios, is presented. It is enabled by the long-range wide-area network (LoRaWAN) communication protocol and it is designed to operate buried underground. The effectiveness of the system was already proved within a previous work [16] by performing several UG2AG transmission series by varying burial depth. On the other hand, in this article, the channel performances are further investigated by considering different soils (i.e., gravel, sand, and clay).

This article is organized as follows. In Section II, some related works on long-range (LoRa) modulation and LoRaWAN protocol for underground networks are reviewed, while in Section III, a model for estimating path loss for soil–air transmission channel is reported. Section IV shows the experimental setup (i.e., the IoUT sensor node and the LoRaWAN network infrastructure). An analysis of the soils in which tests were conducted is reported in Section V, while transmission tests and relative results are exposed in Section VI along with the estimates of path losses given by the application of the path loss model to the test cases, whereas their discussion is outlined in Section VII. Eventually, conclusions and final remarks are highlighted in Section VIII.

II. Related Works

Due to the rapid growth of its popularity, LoRa technology has been tested and employed in a wide range of different application scenarios. Besides its almost traditional use for distributed monitoring infrastructures in urban or rural context, its functioning and reliability have also been tested in critical

Manuscript received July 26, 2020; revised February 3, 2021; accepted February 17, 2021. Date of publication February 24, 2021; date of current version March 12, 2021. The Associate Editor coordinating the review process was Jingyu Hua. *(Corresponding author: Alessandro Pozzebon.)*

Gabriele Di Renzone, Stefano Parrino, Giacomo Peruzzi, and Alessandro Pozzebon are with the Department of Information Engineering and Mathematics, University of Siena, 53100 Siena, Italy (e-mail: gabriele.direnzon@student.unisi.it; parrino2@unisi.it; peruzzi@diism.unisi.it; alessandro.pozzebon@unisi.it).

Duccio Bertoni is with the Department of Earth Sciences, University of Pisa, 56126 Pisa, Italy (e-mail: duccio.bertoni@unipi.it).

Digital Object Identifier 10.1109/TIM.2021.3061820

scenarios such as the monitoring of underground sites [17] or hostile environments such as the marine ones [18].

One of the most critical scenarios is the underground one [19], [20]; in this context, LoRa may be useful, for example, to collect data from underground structures within a smart city scenario [8], [21] or soil features in smart agriculture applications [15]. Nevertheless, despite its importance in different contexts, few papers discussed the reliability of LoRa when transmitting from underground.

The reliability of LoRa modulation in conditions in which nodes are at the edge of their communication range was proved even in underground settings by exploiting communication parameters that speed up the data rate rather than slow it down with setting, which would theoretically ensure better link quality [23].

From simulations on LoRa underground transmissions, a dependence of communication performances on soil moisture content was highlighted and it was also observed that other comparable cellular technologies (e.g., NB-IoT) theoretically outperform LoRa [7]. However, bearing in mind a massive deployment of IoUT sensor nodes, adopting LoRa may reduce either running or fixed cost. Moreover, signal attenuation due to soil moisture may be exploited to detect volumetric water content (VWC) variations by means of a multidimensional deployment of LoRa underground sensor nodes [11].

LoRa UG2UG and UG2AG communications where underground sensor nodes were placed either under manholes in a smart city context [8] or under fields in smart agriculture frameworks [15] were investigated. On the other hand, UG2UG LoRa links under sandy and loam soil were tested [24] even by varying the VWC, burial depth, and covered distance [25], [26]. Such studies confirmed the modulation practicability in those circumstances.

Underground infrastructures (e.g., manholes in urban scenarios) may be suitable for a monitoring system based on synchronous LoRa mesh networks of IoUT sensor nodes in which measurements are forwarded via UG2UG multihop links and bridged to the surface via a UG2AG transmission and then sent via LoRaWAN uplinks to a remote gateway [21].

The quality of UG2AG links enabled by LoRaWAN can be assessed by varying the burial depth of the transmitter [27]; notwithstanding the significant reduction of the received signal strength indicator (RSSI) and the signal-to-noise ratio (SNR) with the increase of the burial depth, satisfactory results were experienced, thus pointing out the robustness of LoRa.

III. Path Loss Model for Soil–Air Transmission Channel

Many articles investigated electromagnetic waves propagation underground analyzing dependencies on soil composition and VWC [28]–[31] or estimating impulse response of such a medium [32]. Other studies performed evaluations on path loss related to underground wireless links [9], [12], [33]–[36], and hereinafter, a similar investigation is conducted for UG2AG transmissions. For the sake of clarity, refer to the model in Fig. 1. Path loss can be calculated by modifying the

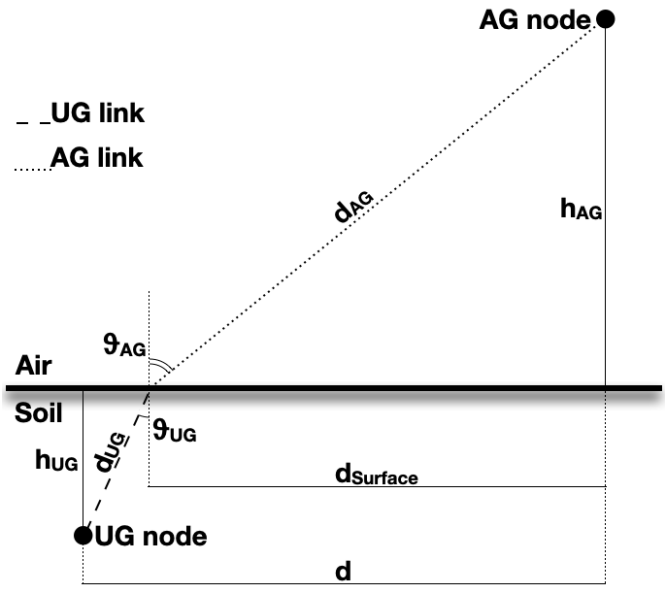

Fig. 1. Channel model for UG2AG links.

Friis formula, i.e., the following equation:

$$P_{RX} = P_{TX} + G_{TX} + G_{RX} - L_{UG} - L_{UG-AG} + -0.5(L_{AG} + L_{Surface}) - L_M - 10\log_{10}(\chi^2) \quad (1)$$

where P_{RX} is the RSSI, P_{TX} is the transmitted power output, G_{TX} is the transmitter antenna gain, G_{RX} is the receiver antenna gain, L_{UG} accounts for underground losses, L_{UG-AG} refers to refraction losses at the soil–air interface, L_{AG} represents aboveground losses, $L_{Surface}$ is the attenuation due to lateral waves, and L_M refers to miscellaneous losses due to sundry possible sources (e.g., obstructions within the first Fresnel zone, antennas polarization mismatch, and so on) and due to the fact that some of the conditions under which the Friis equation can be applied could not be met. Indeed, while the distance between the antennas can be far greater than the carrier wavelength for the most part of UG2AG transmissions, the transmitting and receiving antennas may have different polarizations and they can be probably misaligned. Moreover, due to the fact the transmitting antenna is buried underground, unobstructed free-space hypothesis can never be satisfied. Finally, $10\log_{10}(\chi^2)$ is the path loss due to multipath fading phenomenon.

The aboveground losses L_{AG} may be calculated as free-space loss

$$L_{AG} = 32.45 + 20\log_{10}(d_{AG}) + 20\log_{10}(f) \quad (2)$$

where d_{AG} is the path the signal travels aboveground expressed in km and f is the carrier frequency expressed in MHz. L_{UG} may be computed as suggested in [36] and [37]

$$L_{UG} = 6.4 + 20\log_{10}(d_{UG}) + 20\log_{10}(\beta) + 8.69\alpha d_{UG} \quad (3)$$

where d_{UG} is the path that the signal covers underground expressed in m, α is the attenuation constant, and β is the phase shifting constant. The former two terms may be

evaluated as

$$\alpha = 2\pi f \sqrt{\frac{\mu_0 \mu_r \epsilon_0 \epsilon'}{2}\left[\sqrt{1+\left(\frac{\epsilon''}{\epsilon'}\right)^2}-1\right]} \tag{4}$$

$$\beta = 2\pi f \sqrt{\frac{\mu_0 \mu_r \epsilon_0 \epsilon'}{2}\left[\sqrt{1+\left(\frac{\epsilon''}{\epsilon'}\right)^2}+1\right]} \tag{5}$$

in which f is the carrier frequency, μ_r is the relative magnetic permeability of soil that can be approximated as 1 supposing that the soil composition is metal-free, and ϵ' and ϵ'' are in turn the real and imaginary parts of the effective soil permittivity that can be computed as suggested in [38], respectively. In particular, they can be evaluated by resorting to the mineralogy-based soil dielectric model (MBSDM) [39], which is valid within the range $0.045 \div 26.5$ GHz. It requires as inputs the VWC (V), the carrier frequency, and the percentage of clay (C) related to soil composition. In so doing, the real and imaginary parts of soil permittivity (i.e., ϵ' and ϵ'') are derived from the refractive index n and the normalized attenuation coefficient k as follows:

$$\epsilon' = n^2 - k^2 \tag{6}$$

$$\epsilon'' = 2nk \tag{7}$$

$$n = \begin{cases} n_d + (n_b - 1)V, & \text{if } V < V_m \\ n_d + (n_b - 1)V_m + (n_f - 1)(V - V_m), & \text{else} \end{cases} \tag{8}$$

$$k = \begin{cases} k_d + k_b V, & \text{if } V < V_m \\ k_d + k_b V_m + k_f (V - V_m), & \text{else} \end{cases} \tag{9}$$

where $n_{d,b,f}$ is the refractive index, respectively, of dry soil, bound, and free water; $k_{d,b,f}$ is the normalized attenuation coefficient in turn of dry soil, bound, and free water; and V_m is the maximum bound free water fraction used to distinguish the two moisture regions (i.e., bound and free water). These quantities are evaluated according to

$$n_d = 1.634 - 0.539 \times 10^{-2} C + 0.2748 \times 10^{-4} C^2 \tag{10}$$

$$k_d = 0.03952 - 0.04038 \times 10^{-2} C \tag{11}$$

$$n_{b,f}\sqrt{2} = \sqrt{\sqrt{\left(\epsilon'_{b,f}\right)^2 + \left(\epsilon''_{b,f}\right)^2} + \epsilon'_{b,f}} \tag{12}$$

$$k_{b,f}\sqrt{2} = \sqrt{\sqrt{\left(\epsilon'_{b,f}\right)^2 + \left(\epsilon''_{b,f}\right)^2} - \epsilon'_{b,f}} \tag{13}$$

$$V_m = 0.02863 + 0.30673 \times 10^{-2} C \tag{14}$$

where $\epsilon_{b,f}$ are the complex dielectric values for bound and free water, respectively. The latter ones can be computed as

$$\epsilon'_{b,f} = \epsilon_\infty + \frac{\epsilon_{0b,0f} - \epsilon_\infty}{1 + \left(2\pi f \tau_{b,f}\right)^2} \tag{15}$$

$$\epsilon''_{b,f} = \frac{\epsilon_{0b,0f} - \epsilon_\infty}{1 + \left(2\pi f \tau_{b,f}\right)^2} 2\pi f \tau_{b,f} + \frac{\sigma_{b,f}}{2\pi f \epsilon_0} \tag{16}$$

where $\epsilon_\infty = 4.9$ is the dielectric constant in the high-frequency limit, $\epsilon_{0b,0f}$ are low-frequency limit of the dielectric constant of bound and free water and in particular $\epsilon_{0f} = 100$, $\tau_{b,f}$ are the relaxation time of bound and free water and in particular $\tau_f = 8.5 \times 10^{-12}$, and $\sigma_{b,f}$ are the conductivity, respectively, of bound and free water. Finally, the remaining parameters can be evaluated as follows:

$$\epsilon_{0b} = 79.8 - 85.4 \times 10^{-2} C + 32.7 \times 10^{-4} C^2 \tag{17}$$

$$\tau_b = 1.062 \times 10^{-11} + 3.450 \times 10^{-14} C \tag{18}$$

$$\sigma_b = 0.3112 + 0.467 \times 10^{-2} C \tag{19}$$

$$\sigma_f = 0.3631 + 1.217 \times 10^{-2} C. \tag{20}$$

Alternatively, the real and imaginary parts of soil permittivity may be computed by resorting to the methods and equations presented by the International Telecommunication Union (ITU) in [40]. In particular, for what concerns soils, such model requires the carrier frequency, the temperature, the percentages of either sand or clay, the specific gravity (SG) (i.e., the mass density of the soil sample divided by the mass density of the amount of water in the sample), the VWC, and the bulk density (BD) of the soil samples.

Refraction losses occurring at the soil–air interface are computed as

$$L_{\text{UG-AG}} \simeq 10 \log_{10}\left[\frac{\left(\sqrt{\epsilon'}+1\right)^2}{4\sqrt{\epsilon'}}\right] \tag{21}$$

while the attenuation due to lateral waves is

$$L_{\text{Surface}} = 40 \log_{10}(d_{\text{Surface}}) \tag{22}$$

where d_{Surface} is the distance of the soil–air interface propagation.

Finally, χ is a random variable accounting for path losses due to multipath fading having a Rayleigh distribution

$$f(\chi) = \frac{\chi}{\sigma_R^2} e^{-\frac{\chi^2}{2\sigma_R^2}} \tag{23}$$

where $\sigma_R = (2/\pi)^{1/2}$ is the distribution parameter.

Due to the higher soil permittivity, in comparison with the one of the air, reflected and refracted signals are incident to soil surface. In other words, only signals having small incident angle θ_{UG} are able to emerge toward the surface. Hence, especially for UG2AG links, signals propagate vertically through the soil allowing the approximation $\theta_{\text{UG}} \simeq 0$ that entails either $d_{\text{UG}} \simeq h_{\text{UG}}$ (i.e., the burial depth h_{UG}) or $d_{\text{AG}} = (d^2 + {h_{\text{AG}}}^2)^{1/2}$.

IV. Experimental Setup

Since the aim of this work is to test and analyze the performances of UG2AG LoRaWAN transmissions, a general-purpose LoRaWAN board was exploited as IoUT sensor node. In particular, the B-L072Z-LRWAN1 discovery kit board produced by STMicroelectronics [41] was chosen. It basically embeds an STM32L072CZ microcontroller [42] manufactured by STMicroelectronics and an SX1276 LoRa transceiver [43] constructed by Semtech along with miscellaneous electronics. Concerning its power supply, a power bank was employed, while transmissions were carried out by exploiting a $\lambda/8$ whip antenna having 2 dBi gain that was directly connected to the B-L072Z-LRWAN1 discovery kit board via a Sub Miniature version A (SMA) connector;

TABLE I
RESULTS OF THE SEDIMENTOLOGICAL ANALYSIS PERFORMED ON THE THREE SAMPLES

Sample	Mean $[mm]$	Sorting [Φ]	Coarse Fraction (Gravel) [%]	Medium Fraction (Sand) [%]	Fine Fraction (Clay) [%]
Merse #1	7.126	1.500	86	14	0
Merse #2	0.922	0.734	5	95	0
Certosa	0.056	0.545	3	7	90

such a choice was justified by the study that was worked out during the previous work. Finally, the IoUT sensor node and its antenna were housed within an IP56 box so to protect them during underground trials. The microcontroller runs a firmware implementing a LoRaWAN end device (i.e., a Class A device) sending packets to a gateway on a periodic basis establishing a frequency diversity scheme amid eight different channels in the $863 \div 870$ MHz industrial, scientific, and medical (ISM) band (i.e., 867.1, 867.3, 867.5, 867.7, 867.9, 868.1, 868.3, and 868.5 MHz).

The back end of LoRaWAN network infrastructure enabling the test is the same as the one in [18], while a different gateway was adopted. The latter is an LG308 produced by Dragino [44], which embeds two SX1257 [45] (i.e., LoRa transceivers) and one SX1301 [46] (i.e., a LoRa modem), both produced by Semtech. The gateway has a sensitivity that varies in function of the spreading factor (SF) and the exploited bandwidth for the transmissions. Supposing to employ a bandwidth of 125 kHz, the gateway sensitivity spans from -137 dBm at SF $= 12$ to -126 dBm at SF $= 7$. During the tests, it was equipped with the same antenna as one of the sensor nodes (i.e., a $\lambda/8$ whip antenna having 2 dBi gain). It behaves as a packet forwarder; hence, it first receives and demodulates LoRaWAN packets, and then, it sends such data to a remote network server exploiting the message queuing telemetry transport (MQTT) protocol. The network server was especially designed and implemented by making use of Node-RED. It manages all the incoming packets and stores all the related data (e.g., payloads) and metadata (e.g., RSSIs and SNRs) in a MySQL database.

V. SOIL ANALYSIS

Three deposits have been selected in the surroundings of the city of Siena, Italy, to test the technological solution here proposed, in order to check the efficiency under various conditions. In particular, the main difference is represented by the grain size, which significantly differs from sample to sample and accounts for different behaviors and properties (e.g., angle of repose, packing, permeability, organic matter content, and so on). Therefore, we elected to analyze three samples constituted by gravel, sand, and clay as representative of pure soils. From a geological point of view, such choice makes sense because they exemplify the three main grain-size classes in which sedimentologic scales are classified (e.g., Wentworth scale [48]). Nonetheless, it is also useful because the vast majority of agricultural soils are usually composed of a combination of such grain-size classes: knowledge about the behavior of pure soils would help predicting the behavior of mixed soils.

The first two samples have been collected from an emerged longitudinal bar along the Merse river bed (i.e., samples Merse #1 and Merse #2). Due to the strong flows that typically characterize such a stream, the deposits were expected to be characteristically devoid of fine particles (<63 μm), which would be easily washed away with no chance of deposition in such environment. As the sampling site along the river is located far from the alluvial plain, here, the river still maintains the flow characteristics of a mountain creek. Gravel accumulations have been easily spotted along the riverbed, as well as sand deposits. The clay sample has been collected further downstream, in a site characterized by frequent floods over the natural levee. Such alluvial deposits are usually constituted by finest particles, as coarser sediments can hardly be transported past the levee even during flooding events.

The sedimentological characterization of the three samples has been carried out to calculate the traditional parameters that best define the main properties of sediments. Such parameters are mean and sorting [47], and the percentage of coarse (>2 mm, gravel), medium (from 2 mm to 63 μm, sand), and fine (<63 μm, clay) fractions. Mean corresponds to the average grain size of the sample; sorting describes the heterogeneity of the grain sizes comprised in the sample. Percentage of coarse, medium, and fine fractions is the proportion between the main populations of sediment grain sizes in accordance with the Wentworth scale [48]. About 1 kg of sediment was sampled from the selected sites, collecting with a small shovel the surface of the deposits. The laboratory analysis was carried out in accordance with the technique described in [49]. No further characterization of the finest population has been done. The resulting data (see Table I) were processed with an Excel macro named Granu, which enabled the calculation of the textural parameters.

The results of the grain-size analysis confirmed the expectations, as the first two samples (i.e., Merse #1 and Merse #2) present no fine fraction, and varying content of coarse and medium fractions. The coarser one (i.e., Merse #1) is characterized by 86% of gravel and pebbles, which translates to a 7.126 mm mean grain size. Merse #2 is almost entirely constituted by sand (i.e., 95%), with a mean grain size of 0.922 mm (i.e., medium sand). Though the percentage of sand is almost 100%, the sorting is moderately poor (i.e., 0.734), meaning that Merse #2 sample includes very fine to very coarse sands. Merse #1 sorting is poor, as expected in a sample characterized by such proportions of coarse and medium fractions. The Certosa sample confirms the provenance from the "Crete Senesi" deposit, as the mean grain size is well below the 63 μm threshold between fine and medium particles

Fig. 2. Soil samples used for the gravimetric analysis: from left to right, Merse #2, Merse #1, and Certosa; and from top to bottom their pick depth, 10, 30, and 50 cm.

(i.e., 0.056 mm); predictably, such sample is very well sorted (i.e., 0.545).

Following the sedimentological characterization, a gravimetric analysis was carried out on soil samples to measure their VWC and BD. In particular, soil samples were collected at three depths, i.e., 10, 30, and 50 cm; since differences among these depths are very small, intermediate values may be easily derived by interpolation. Moreover, the limited difference does not justify a finer gravimetric analysis that considers other depths in between the considered ones. An image of the nine soil samples after gravimetric analysis can be seen in Fig. 2: from left to right shown samples are Merse #2, Merse #1, and Certosa, and samples were displaced according to their pick depth starting from 10 cm at the bottom and 50 cm at the top.

Concerning the gravimetric analysis, as soon as the nine samples were collected, they were placed in a container of known weight and volume V_{tot} and then weighted with a scale featuring a 0.001-g degree of precision. The samples were then put inside an oven, at a temperature of 105 °C: their weight was then checked every 12 h. When the difference among two consecutive measurements was lower than 0.01 g, the samples were assumed to be dry. VWC and BD were then calculated by applying the following formulas:

$$\text{VWC} = \frac{V_{\text{water}}}{V_{\text{tot}}} = \frac{m_{\text{wet}} - m_{\text{dry}}}{\rho_{\text{water}} V_{\text{tot}}} \tag{24}$$

$$\text{BD} = \frac{m_{\text{dry}}}{V_{\text{tot}}} \tag{25}$$

where m_{wet} is the mass of wet soil and m_{dry} is the mass after being dried in the oven, while water density ρ_{water} has been assumed as equal to 1 g/cm^3. Concerning the SG, this has not been measured since standard values can be found in the literature [50]. Notice that variations according to different soil compositions are very small; therefore, for sand and gravel soils, an SG of 2.66 was chosen, whereas an SG of 2.56 was considered for clay. All the values can be seen in Table II, where all the measured data are presented.

TABLE II
RESULTS OF THE GRAVIMETRIC ANALYSIS PERFORMED ON THE THREE SAMPLES

Measurement	Sample	Burial Depth $[cm]$		
		10	30	50
VWC [%]	Merse #1	7.15	9.35	9.74
	Merse #2	5.67	6.37	7.26
	Certosa	28.80	31.14	29.99
BD $[g/cm^3]$	Merse #1	1.45	1.54	1.39
	Merse #2	1.23	1.20	1.22
	Certosa	1.28	1.45	1.34
SG	Merse #1	2.66	2.66	2.66
	Merse #2	2.66	2.66	2.66
	Certosa	2.56	2.56	2.56

VI. TESTS AND RESULTS

Once that the soils were identified and analyzed, tests on UG2AG transmissions were carried out so to apply the theoretical concepts introduced in Section III to each of the test arrangements.

The following factors were considered while defining the experimental setup:

1) the possible RSSI degradation in long-lasting operations due to the soil compaction;
2) the different achievable results when placing the receiver at different distances from the transmitter;
3) the attenuation due to different salinity levels in soil.

For what concerns the first point, a preliminary test was carried out so to demonstrate the lack of influence of soil compaction on RSSI. Regarding the other two points, these were faced when defining the final experimental setup for the field tests.

A. Preliminary Test

The aim of this test was to demonstrate that the actual compaction of soil has no impact on the RSSI; this result is crucial to show the validity of the data collected during the field tests since these were performed with the node buried under a layer of soil manually compacted, starting the data acquisition phase immediately after the node burial, without the need to wait for the soil compaction.

The preliminary test was carried out burying a node in a soil characterized by a mixed composition: sedimentological analysis results for this soil pointed out that it is made by 9% of gravel, 26% of sand, and 65% of clay, while it has a mean of 0.112 mm and a sorting of 2.0 Φ. Such a composition was chosen in order to detect possible attenuation contribution for every kind of soil since the sample has a sundry makeup.

Since the aim of this test was only to detect possible decreases in the RSSI due to soil composition, a single SF was chosen for all the transmissions (i.e., SF = 12); indeed, RSSI is not dependent on the SF which, on the other hand, has a notable impact on packet loss (PL) because it decreases the receiver sensitivity. Similarly, no particular assumption was made for what concerns soil salinity and distance from transmitter and receiver; in particular, the gateway was indoor placed at a 27-m distance from the transmitter. The node was buried at a 30-cm depth and covered by paying attention to

Fig. 3. Compacted soil surface after node burial for the preliminary test.

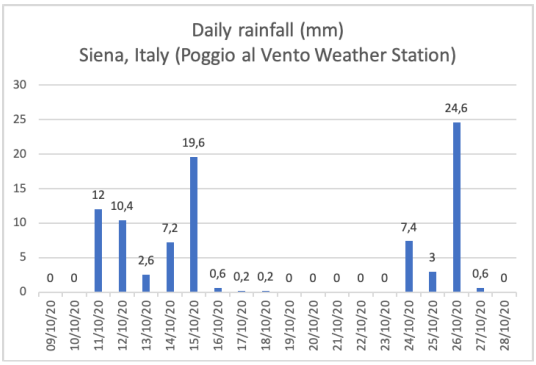

Fig. 4. Daily rainfalls during the 20 days of the preliminary test.

compacting the soil (Fig. 3 shows the compacted soil surface after node burial) and then kept in transmission for 20 days, with a transmission rate of one packet every 20 min. During this time span, different weather conditions were experienced, from clear sky to heavy rains; daily rainfalls (see Fig. 4) were retrieved from the closest weather station which located at 2.2 km far from the test site (i.e., Poggio al Vento weather station). The alternation between rainy and sunny periods allowed full compaction of the soil after around ten days.

Fig. 5 shows the trends of RSSI and SNR for the 20 days time span by plotting their moving averages both having a 3-h window. From the figure, it is evident that the soil compaction has no effect on the actual transmission performances for the LoRaWAN channel. Indeed, there is no sign of any decrease for the two parameters, in particular for RSSI, along the whole 20 days period. Periodic fluctuations that can be noticed in the trends are not correlated with rainfalls (see Fig. 4) and consequently with soil moisture, and they may be due to a wealth of other factors that are difficult to be considered. Nevertheless, the RSSI value is always in a range of $-93 \div -109$ dBm, with a mean value of -100.47 dBm. On the other hand, SNR spans in the range of $9 \div 1$ dB with a mean value of 5.80 dB. These results suggest that reliable data can be collected regardless of either the degree of soil compaction or the time the node spends buried underground.

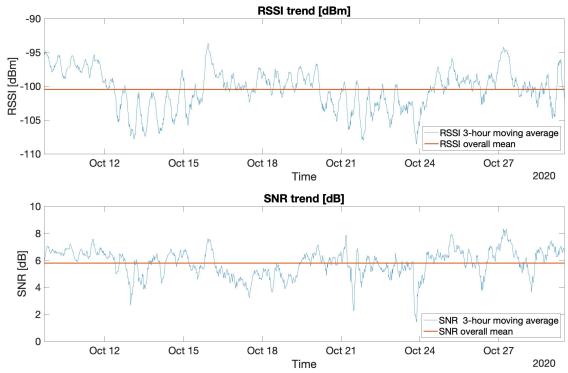

Fig. 5. Preliminary test results: RSSI and SNR trends.

B. Field Tests

Field tests were carried out in the three sites described in Section V: Fig. 6 shows the IoUT sensor node during the burial depth measurement phase, just before its covering with soil, within gravel soil. Such a test was performed bearing in mind the following assumptions.

1) The sites were chosen in a fluvial environment, in order to reduce as much as possible the attenuating effects due to salinity, since fluvial soils are characterized by negligible salinity levels. While the effect of this parameter should also be considered, the aim of this article is to discuss the transmission performances in different types of soils from a sedimentological point of view. A characterization according to the soil chemical composition, even if interesting, is out of the scope of this article since it would require a different approach and different typologies of tests.
2) For each soil, tests were performed at five burial depths (i.e., 10, 20, 30, 40, and 50 cm). No tests were performed at greater depths since a large part of significant underground monitoring applications are deployed at a maximum depth of 50 cm: for instance, in works like [51]–[55] that deal with various application scenarios (i.e., smart farming, smart agriculture, pipeline monitoring, and underground monitoring in a broad sense), sensor nodes were not buried at bigger depths. Moreover, for greater depths, the actual functioning of the LoRaWAN network can be assessed by considering the underground attenuation models and combining them with the experimental results presented hereinafter.
3) For each of the trials, the soil was thoroughly compacted so to uniform soil density after the node burial. Such a procedure was performed just in order to reduce the number of involved variables within the experimentation since the preliminary test showed that soil compaction does not notably affect communication performances.
4) Concerning the radio settings, a power output of 14 dBm, a coding rate (CR) of 4/5, and a bandwidth of 125 kHz were chosen. For what concerns the SF, since this parameter is crucial to identify the best tradeoff among PL and power consumption, tests were performed

TABLE III

UNDERGROUND TESTS RESULTS: RSSIS AND SNRS MEASURED VALUES AND RELATIVE UNCERTAINTIES ALONG WITH PLS FOR GRAVEL SOIL (MERSE #1)

			Burial Depth $[cm]$				
			10	20	30	40	50
SF=7	RSSI $[dBm]$	$\bar{x}$	-80.6	-82.1	-85.1	-93.2	-92.9
		$u_c(\bar{x})$	0.6	0.6	0.6	0.6	0.6
	SNR $[dB]$	$\bar{x}$	8.7	9.0	8.6	5.2	3.2
		$u_c(\bar{x})$	0.1	0.1	0.1	0.3	0.2
	PL $[\%]$		0.6	0	0	0	0
SF=8	RSSI $[dBm]$	$\bar{x}$	-80.9	-82.6	-83.7	-92.8	-93.0
		$u_c(\bar{x})$	0.6	0.6	0.6	0.6	0.6
	SNR $[dB]$	$\bar{x}$	10.2	10.1	10.5	7.0	3.7
		$u_c(\bar{x})$	0.1	0.1	0.1	0.3	0.2
	PL $[\%]$		0	0	0	0	0
SF=9	RSSI $[dBm]$	$\bar{x}$	-82.4	-84.3	-85.1	-94.7	-94.5
		$u_c(\bar{x})$	0.6	0.6	0.6	0.6	0.6
	SNR $[dB]$	$\bar{x}$	11.4	11.1	10.8	3.0	3.5
		$u_c(\bar{x})$	0.2	0.2	0.1	0.4	0.2
	PL $[\%]$		1	0	0	0	0
SF=10	RSSI $[dBm]$	$\bar{x}$	-79.2	-80.5	-81.8	-92.7	-92.9
		$u_c(\bar{x})$	0.6	0.6	0.6	0.6	0.6
	SNR $[dB]$	$\bar{x}$	9.6	10.2	10.9	5.2	3.4
		$u_c(\bar{x})$	0.2	0.2	0.1	0.3	0.2
	PL $[\%]$		0	0	0	0	0
SF=11	RSSI $[dBm]$	$\bar{x}$	-80.0	-82.1	-82.6	-94.0	-93.0
		$u_c(\bar{x})$	0.6	0.6	0.6	0.6	0.6
	SNR $[dB]$	$\bar{x}$	11.1	11.1	11.6	4.0	4.5
		$u_c(\bar{x})$	0.1	0.2	0.1	0.3	0.2
	PL $[\%]$		0	0	0	0	0
SF=12	RSSI $[dBm]$	$\bar{x}$	-79.4	-80.8	-82.7	-93.8	-91.6
		$u_c(\bar{x})$	0.6	0.6	0.6	0.6	0.6
	SNR $[dB]$	$\bar{x}$	9.1	9.7	9.2	0.3	3.9
		$u_c(\bar{x})$	0.1	0.1	0.1	0.4	0.2
	PL $[\%]$		0	0.3	0	0	1.6

at each SF allowed by the LoRaWAN protocol (i.e., from 7 to 12).

5) The gateway was placed at a 15-m distance from the burial point and laid on the ground for each measurement. This distance was chosen in order to add a relatively short aboveground transmission distance, thus better identifying the link budget component for the underground segment of the transmission. The tests were not performed at other distances due to the fact that transmission performances at different distances can be easily assessed by considering the behavior of LoRaWAN networks in air, which was discussed in a wealth of papers such as [18] and [56]–[58].

For what concerns data acquisition, the following methodology was sorted out.

1) Three hundred packets having a 10 B payload were sent at each of the burial depths (i.e., 10, 20, 30, 40, and 50 cm), for each SF (i.e., 7, 8, 9, 10, 11 and 12).
2) For each of the received packets, the RSSI and SNR values were sampled and stored.
3) For each of the test groups (i.e., 300 transmissions for a certain SF at a certain depth and within a certain soil), the PL was calculated.

The results of the underground transmission tests are shown in Fig. 7 and Tables III–V. In particular, Fig. 7(a) shows the measured RSSI values and the relative uncertainties by considering as instrumental maximum error the instrument resolution (i.e., 1 dBm) for each of the different experimental settings and the different burial depths, while Fig. 7(b) similarly shows measured SNR values and the relative uncertainties by considering as instrumental maximum error the instrument

Fig. 6. IoUT sensor node during tests. Ropes were used to ease the node retrieval.

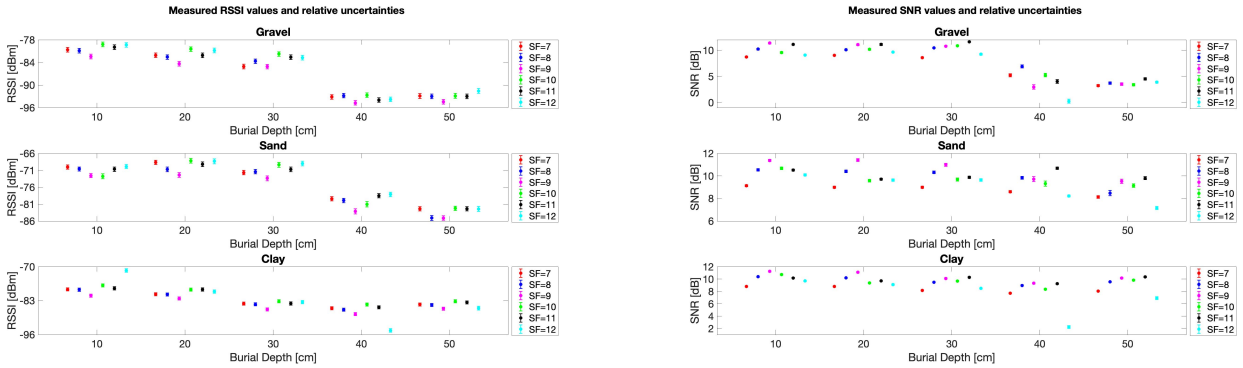

(a) (b)

Fig. 7. Underground tests results. (a) Measured RSSI values and relative uncertainties and (b) measured SNR values and relative uncertainties.

TABLE IV

UNDERGROUND TESTS RESULTS: RSSIS AND SNRS MEASURED VALUES AND RELATIVE UNCERTAINTIES ALONG WITH PLS FOR SAND SOIL (MERSE #2)

			Burial Depth $[cm]$				
			10	20	30	40	50
SF=7	RSSI $[dBm]$	$\bar{x}$	-70.0	-68.6	-71.7	-79.4	-82.4
		$u_c(\bar{x})$	0.6	0.6	0.6	0.6	0.6
	SNR $[dB]$	$\bar{x}$	9.1	9.0	9.0	8.6	8.1
		$u_c(\bar{x})$	0.1	0.1	0.1	0.1	0.1
	PL [%]		0	0	0	0	0
SF=8	RSSI $[dBm]$	$\bar{x}$	-70.6	-70.7	-71.4	-79.9	-85.1
		$u_c(\bar{x})$	0.6	0.7	0.7	0.6	0.7
	SNR $[dB]$	$\bar{x}$	10.5	10.4	10.3	9.8	8.5
		$u_c(\bar{x})$	0.1	0.1	0.1	0.1	0.2
	PL [%]		0	0	0	0	0
SF=9	RSSI $[dBm]$	$\bar{x}$	-72.6	-72.4	-73.4	-83.1	-85.1
		$u_c(\bar{x})$	0.6	0.7	0.7	0.7	0.6
	SNR $[dB]$	$\bar{x}$	11.4	11.4	11.0	9.7	9.5
		$u_c(\bar{x})$	0.1	0.1	0.1	0.2	0.2
	PL [%]		0.3	0	0	0	0
SF=10	RSSI $[dBm]$	$\bar{x}$	-72.8	-68.2	-69.4	-81.0	-82.2
		$u_c(\bar{x})$	0.7	0.7	0.7	0.8	0.6
	SNR $[dB]$	$\bar{x}$	10.7	9.6	9.7	9.3	9.1
		$u_c(\bar{x})$	0.1	0.1	0.1	0.2	0.1
	PL [%]		0	0	0	0	0
SF=11	RSSI $[dBm]$	$\bar{x}$	-70.7	-69.2	-70.8	-78.5	-82.4
		$u_c(\bar{x})$	0.6	0.7	0.7	0.6	0.6
	SNR $[dB]$	$\bar{x}$	10.5	9.7	9.9	10.7	9.8
		$u_c(\bar{x})$	0.1	0.1	0.1	0.1	0.1
	PL [%]		0	0	0	0	0
SF=12	RSSI $[dBm]$	$\bar{x}$	-69.9	-68.3	-69.0	-78.1	-82.4
		$u_c(\bar{x})$	0.6	0.7	0.7	0.6	0.7
	SNR $[dB]$	$\bar{x}$	10.1	9.6	9.6	8.2	7.2
		$u_c(\bar{x})$	0.1	0.1	0.1	0.1	0.1
	PL [%]		0	0	0	0	0

resolution (i.e., 0.01 dB). The detailed numerical results for each soil are then shown in Tables III–V that also include data on PLs.

C. Path Loss Estimation

Let us apply the model described in Section III. Since the IoUT sensor node implements a frequency diversity scheme, the mean value of the frequencies of the channels (i.e., 867.8 MHz) will be involved in all the equations. As it was previously stated, the gateway was placed at a distance d_{AG} of 15 m, due to the fact that it was laid on the ground, $d_{\text{Surface}} = d_{\text{AG}}$. Therefore, from (2), L_{AG} is equal to 54.74 dB, and, from (22), L_{Surface} is equal to 47.04 dB. For what concerns the remainder terms of (1), they vary depending on the adopted procedure to evaluate ϵ' and ϵ'' (i.e., according to MBSDM and ITU). In particular, the ITU method was carried out by resorting to a specific MATLAB function [59].

TABLE V

UNDERGROUND TESTS RESULTS: RSSIS AND SNRS MEASURED VALUES AND RELATIVE UNCERTAINTIES ALONG WITH PLS FOR CLAY SOIL (CERTOSA)

			Burial Depth $[cm]$				
			10	20	30	40	50
SF=7	RSSI $[dBm]$	$\bar{x}$	-78.7	-80.5	-84.1	-85.9	-84.5
		$u_c(\bar{x})$	0.6	0.6	0.6	0.6	0.6
	SNR $[dB]$	$\bar{x}$	8.8	8.8	8.2	7.7	8.1
		$u_c(\bar{x})$	0.1	0.1	0.1	0.1	0.1
	PL [%]		0.6	0	1	0.3	0.3
SF=8	RSSI $[dBm]$	$\bar{x}$	-78.8	-80.6	-84.4	-86.5	-84.6
		$u_c(\bar{x})$	0.6	0.6	0.6	0.6	0.6
	SNR $[dB]$	$\bar{x}$	10.4	10.2	9.5	9.0	9.6
		$u_c(\bar{x})$	0.1	0.1	0.1	0.1	0.1
	PL [%]		0.3	0	0.3	0.3	0.3
SF=9	RSSI $[dBm]$	$\bar{x}$	-81.1	-82.2	-86.3	-88.2	-86.1
		$u_c(\bar{x})$	0.6	0.6	0.6	0.6	0.6
	SNR $[dB]$	$\bar{x}$	11.3	11.1	10.1	9.3	10.2
		$u_c(\bar{x})$	0.1	0.1	0.1	0.1	0.1
	PL [%]		0.6	0.3	1	1	0.3
SF=10	RSSI $[dBm]$	$\bar{x}$	-77.1	-78.8	-82.2	84.5	-83.2
		$u_c(\bar{x})$	0.6	0.6	0.6	0.6	0.6
	SNR $[dB]$	$\bar{x}$	10.7	9.4	9.7	8.4	9.8
		$u_c(\bar{x})$	0.1	0.1	0.1	0.1	0.1
	PL [%]		0.6	0.3	0.3	1	0
SF=11	RSSI $[dBm]$	$\bar{x}$	-78.3	-78.7	-84.1	-85.5	-83.7
		$u_c(\bar{x})$	0.6	0.6	0.6	0.6	0.6
	SNR $[dB]$	$\bar{x}$	10.2	9.7	10.3	9.2	10.4
		$u_c(\bar{x})$	0.1	0.1	0.1	0.1	0.1
	PL [%]		0	1	0.3	0	1.6
SF=12	RSSI $[dBm]$	$\bar{x}$	-71.5	-79.5	-83.5	-94.4	-85.9
		$u_c(\bar{x})$	0.7	0.6	0.6	0.6	0.7
	SNR $[dB]$	$\bar{x}$	9.7	9.1	8.5	2.2	6.9
		$u_c(\bar{x})$	0.1	0.1	0.1	0.2	0.2
	PL [%]		0.3	6	0	3.3	6.6

TABLE VI

RESULTS OF (4) AND (5) EXPLOITING THE VALUES OF ϵ' AND ϵ'' EITHER ACCORDING TO MBSDM OR ITU MODEL FOR GRAVEL SOIL (MERSE #1)

Burial Depth $[cm]$	MBSDM				ITU			
	$\epsilon^{'}$ $[F/m]$	$\epsilon^{''}$ $[F/m]$	α $[1/m]$	β $[rad/m]$	$\epsilon^{'}$ $[F/m]$	$\epsilon^{''}$ $[F/m]$	α $[1/m]$	β $[rad/m]$
10	5.04	0.37	1.58	40.87	3.83	0.41	1.88	35.62
30	5.97	0.47	1.72	44.67	4.49	0.56	2.39	38.61
50	6.14	0.48	1.75	45.11	4.56	0.53	2.25	38.89

TABLE VII

RESULTS OF (4) AND (5) EXPLOITING THE VALUES OF ϵ' AND ϵ'' EITHER ACCORDING TO MBSDM OR ITU MODEL FOR SAND SOIL (MERSE #2)

Burial Depth $[cm]$	MBSDM				ITU			
	$\epsilon^{'}$ $[F/m]$	$\epsilon^{''}$ $[F/m]$	α $[1/m]$	β $[rad/m]$	$\epsilon^{'}$ $[F/m]$	$\epsilon^{''}$ $[F/m]$	α $[1/m]$	β $[rad/m]$
10	4.46	0.31	1.38	38.44	12.12	2.96	7.67	63.76
30	4.73	0.34	1.42	39.59	12.90	3.22	8.09	65.81
50	5.09	0.37	1.47	41.05	13.47	3.12	7.69	67.18

In addition, they also change in compliance with the burial depth because the required parameters by the two models change by following the same fashion. Therefore, the values of ϵ' and ϵ'' along with the results from (4) and (5) are reported within Tables VI–VIII either for MBSDM or ITU procedure and, respectively, for the three test soils.

Finally, the RSSIs estimates may be computed by applying (1), and the results are tallied within Table IX. For the sake of comparison, for each of test site, the mean values of RSSIs were computed by averaging the sampled data for all of the SF at the burial depth of 10, 30, and 50 cm, and also, these values are listed in Table IX.

VII. DISCUSSION

While some of the results and outcomes discussed in this section were already presented in other papers, as far as we are concerned, no work was previously done that focuses in detail on LoRaWAN performances in different soils featuring

TABLE VIII
RESULTS OF (4) AND (5) EXPLOITING THE VALUES OF ϵ' AND ϵ'' EITHER ACCORDING TO MBSDM OR ITU MODEL FOR CLAY SOIL (CERTOSA)

Burial Depth $[cm]$	MBSDM				ITU			
	$\epsilon^{'}$ $[F/m]$	$\epsilon^{''}$ $[F/m]$	α $[1/m]$	β $[rad/m]$	$\epsilon^{'}$ $[F/m]$	$\epsilon^{''}$ $[F/m]$	α $[1/m]$	β $[rad/m]$
10	6.71	2.29	7.96	47.77	9.71	2.09	6.07	57.00
30	7.84	2.70	8.61	51.64	11.59	2.48	6.59	62.26
50	7.27	2.49	8.29	49.74	10.55	2.27	6.32	59.38

TABLE IX
RSSIS ESTIMATES BY APPLYING THE MODEL IN SECTION III EVALUATING ϵ' AND ϵ'' EITHER ACCORDING TO MBSDM OR ITU MODEL IN COMPARISON WITH THE MEAN VALUES OF THE MEASURED RSSIS

Burial Depth $[cm]$	RSSI estimates $[dBm]$						RSSI mean measurements $[dBm]$		
	MBSDM			ITU					
	Gravel (Merse #1)	Sand (Merse #2)	Clay (Certosa)	Gravel (Merse #1)	Sand (Merse #2)	Clay (Certosa)	Gravel (Merse #1)	Sand (Merse #2)	Clay (Certosa)
10	-54.03	-53.36	-60.86	-53.16	-62.99	-60.67	-80.4	-71.1	-77.6
30	-67.38	-65.65	-86.57	-67.95	-87.22	-82.85	-83.5	-70.9	-85.3
50	-75.04	-73.08	-104.27	-75.99	-104.14	-97.16	-93.0	-83.3	-84.7

pure a sedimentological composition. As a matter of fact, only in [15], the impact of soil composition on transmission performances, even if not for pure soils, was debated. Other papers simply examine underground LoRa transmission, regardless of the type of soil [24], [26], [27], or consider other influence parameters [25].

Considering the results shown in Fig. 7 and Tables III–V, it is possible to make some interesting considerations about the usability of the LoRa technology for data transmission from underground to aboveground in different contexts.

First, we can affirm that successful data transmissions from underground at depths up to 50 cm can be achieved for every soil composition. Indeed, for the proposed experimental setup, for each test, PL was almost always below 2% (apart for clay at SF $= 12$ for depths of 40 and 50 cm), which can be considered a physiological threshold for any successful LoRa transmission. Concerning the different types of soil, results show that gravel provides the worst performances for what concerns RSSI and SNR, while the best ones are provided by sandy soil. Nevertheless, the difference is in general around 10 dBm, suggesting that these values can be used to estimate the performances of the most part of common soils that are in general a mixture of these three particle sizes.

Since LoRa receivers are generally characterized by a very high sensitivity value (e.g., the exploited gateway for this measurement campaign has a sensitivity down to -137 dBm at SF $= 12$), which allows to receive packets even with very poor RSSIs, the results of the test suggest the usability of this transmission technology even in harsher conditions. Nevertheless, the following considerations can be made.

1) In order to better point out the attenuating effects of the UG2AG transmission, for what concerns the underground lag of the transmission channel, the gateway was placed at a limited distance from the node burial spot. Nevertheless, even in the worst case, link margin (LM) is high enough (LM $= -94.7$ dBm $+ 137$ dBm $=$ 42.3 dBm) to ensure a theoretically long aboveground transmission distance. Indeed, at 868 MHz, for a 1000-m transmission distance in air, free-space loss can be calculated as in (2) resulting in 31.22 dBm.
2) Other factors may concur in degrading the transmitted signal, first of all VWC; indeed, for every kind of radio transmission, a larger water presence turns in larger attenuating phenomena. While the assessment of the system performances for different VWC contents falls outside the scope of this article, a rough indication of its possible contribution can be extrapolated from the preliminary test described in Section VI-A; in this case, the node was kept running for a 20-day period, during which several rainy days were experienced. As a consequence, a high VWC was surely experienced in this time span. Nevertheless, no significant signal degradation was experienced, thus suggesting that VWC impact on link budget should be quite limited.
3) Another critical parameter that may affect the UG2AG channel is the chemical composition of soil. In this case, high salinity values or presence of metallic sediments may have attenuating effects on transmission. Analyzing such a phenomenon by means of field tests is anyway very complex because of several factors. Some of them include the difficulty in finding a wide range of different test sites characterized by the required chemical compositions, the wide range of possible parameters to be considered, and the nonhomogeneity of the composition even in soils with homogeneous sedimentological features.

A further analysis points out that RSSIs and SNRs related to 50 cm underground within gravel (i.e., Merse #1) and clay (i.e., Certosa) are slightly better than those obtained at a burial depth of 40 cm within the same fields. These odd data are justified by the fact that LoRaWAN networks are naturally subject to RSSI oscillations at the receiver side (as it can be also noticed in the preliminary test) due to a plethora of factors, the bulk of which are hardly identifiable. By relying on the preliminary test results, it can be concluded that the technology itself and the hardware components intrinsically

cause these variations. Nonetheless, such oscillatory outcomes usually stem out from statistical fluctuations, and thus, they would be averaged out in case a huge number of packets would have been received. Theoretically, the aforesaid number should be infinite, but practically speaking, the same effect (i.e., fluctuation vanishing) would take place whether the number of received packets would have been $3 \div 4$ orders of magnitude greater than the one carried out during the tests. However, since the scope of this article was to validate the technology practical usability within underground settings, carrying out tests aiming at reducing RSSI fluctuations falls outside this article purpose.

A last, important consideration has to been drawn by resorting to data within Tables VI–VIII; from these values, the difference between theoretically calculated and measured RSSI values is evident. Such a result suggests that perfect modeling of a real UG2AG transmission channel is scarcely achievable. The discrepancy among the values may be due to an extremely wide range of different factors, such as the presence of attenuating items in the test environments (e.g., trees, vegetation, river, and so on), different environmental and meteorological conditions during the tests (relative humidity, mist, temperature, and so on), or the possible presence of rock layers below the test sites. All these factors are almost unpredictable and fall within the so-called miscellaneous losses L_M. At the same time, for some tests, the measured value is larger than the theoretical one; in this case too, several factors may concur in achieving this outcome such as, for instance, soil porosity. The aforementioned results could be exploited for modifying the theoretical models in order to derive a finer one. However, this would require additional experimentations that must be conducted within controlled environments (e.g., a laboratory) aimed at varying soil chemical-physical parameters while measuring transmission performances. Indeed, parameters, such as soil composition, BD, salinity, presence of metallic materials, presence of electrolyte within soil, and many others, affect losses within soil medium. For instance, the BD we measured was the one related to a circumscribed neighborhood of the transmitter burial point (i.e., it was measured in a punctual fashion). Maybe, BD related to soil propagating the signals could experience a massive variation, which could translate into one of the effects causing dissimilarities amid estimates and measures. Unfortunately, though, performing a distributed measurement for BD was barely impossible within field tests. In conclusion, despite these discrepancies, it is still possible to point out that the theoretical models can be extremely precious to evaluate the feasibility of the UG2AG radio link, provided that miscellaneous losses (having an order of magnitude that can be deduced from the comparison in Table IX) are considered during estimation procedures.

VIII. Conclusion

The aim of this article was to analyze the behavior of a UG2AG LoRaWAN transmission channel (i.e., a transmitter buried underground and a receiver placed aboveground) in case of different soils. The field tests performed focused on three testing sites featuring three almost pure compositions; in particular, sand, clay, and gravel soils were tested. These compositions were selected since most part of soils is basically a combination of these three grain sizes; this means that once the behavior of the LoRa channel is known in these three conditions, the actual implementation of a working connection in any kind of soil (i.e., a soil composed of different percentages of the three grain-sizes) can be easily deduced if the soil composition is known.

This article mainly focuses on field measurements, performed in real sites whose compositions were analyzed in detail, comparing them with a theoretical analysis of the transmission channel. The values proposed in this article can then be used in the evaluation phase for the feasibility of any kind of buried LoRa-based monitoring system. In this sense, the proposed results may find use in several application scenarios, from environmental monitoring to the monitoring of critical, buried infrastructures such as aqueducts or pipelines.

While the transmission was tested for a depth up to 50 cm, further work may be expected to be carried out to define the system behavior also for greater depths. Nevertheless, the results proposed in this article can be already used to evaluate the operation of the LoRa technology even at different depths with respect to the ones analyzed in this work.

Future works may also include the assessment of PL, SNR, and RSSI in the function of other test parameters such as distance between gateway (even though such quantity moderately impacts on link budget with respect to underground losses) and IoUT sensor node (e.g., 30, 50, 75, and 100 m), VWC and, in particular, chemical composition of the soil including salinity, since such parameter may have a significant influence on the actual transmission performances. In addition, further studies testing LoRaWAN UG2AG links on other frequency bands (e.g., 433 and 915 MHz) may be sorted out, along with the assessment of transmission performances whenever greater burial depths are exploited (e.g., 1 m). Eventually, the discrepancies amid estimates and measures hint further studies and laboratory tests aiming at perfecting the state-of-the-art soil loss models, albeit they can be still deemed to be a reliable and valuable tool for WUSNs planning.

References

[1] I. F. Akyildiz and E. P. Stuntebeck, "Wireless underground sensor networks: Research challenges," *Ad Hoc Netw.*, vol. 4, no. 6, pp. 669–686, Nov. 2006.

[2] A. R. Silva and M. C. Vuran, "Communication with aboveground devices in wireless underground sensor networks: An empirical study," in *Proc. IEEE Int. Conf. Commun.*, May 2010, pp. 1–6.

[3] X. Q. Yu, Z. L. Zhang, and W. T. Han, "Evaluation of communication in wireless underground sensor networks," *IOP Conf. Series, Earth Environ. Sci.*, vol. 69, no. 1, Jun. 2017, Art. no. 012083.

[4] N. Saeed, M. S. Alouini, and T. Y. Al-Naffouri, "Toward the Internet of underground Things: A systematic survey," *IEEE Commun. Surveys Tuts.*, vol. 21, no. 4, pp. 3443–3466, 4th Quart., 2019.

[5] N. Saeed, M.-S. Alouini, and T. Y. Al-Naffouri, "3D localization for Internet of underground things in oil and gas reservoirs," *IEEE Access*, vol. 7, pp. 121769–121780, 2019.

[6] A. Salam, M. C. Vuran, and S. Irmak, "Towards Internet of underground Things in smart lighting: A statistical model of wireless underground channel," in *Proc. IEEE 14th Int. Conf. Netw., Sens. Control (ICNSC)*, May 2017, pp. 574–579.

[7] H. Malik, N. Kandler, M. M. Alam, I. Annus, Y. Le Moullec, and A. Kuusik, "Evaluation of low power wide area network technologies for smart urban drainage systems," in *Proc. IEEE Int. Conf. Environ. Eng. (EE)*, Mar. 2018, pp. 1–5.

[8] S. Kartakis, B. D. Choudhary, A. D. Gluhak, L. Lambrinos, and J. A. McCann, "Demystifying low-power wide-area communications for city IoT applications," in *Proc. 10th ACM Int. Workshop Wireless Netw. Testbeds, Experim. Eval.*, Oct. 2016, pp. 2–8.

[9] D. Du, H. Zhang, J. Yang, and P. Yang, "Propagation characteristics of the underground-to-aboveground communication link about 2.4 GHz and 433 MHz radio wave: An empirical study in the pine forest of Guizhou province," in *Proc. 3rd IEEE Int. Conf. Comput. Commun. (ICCC)*, Dec. 2017, pp. 1041–1045.

[10] M. C. Vuran, A. Salam, R. Wong, and S. Irmak, "Internet of underground Things in precision agriculture: Architecture and technology aspects," *Ad Hoc Netw.*, vol. 81, pp. 160–173, Dec. 2018.

[11] F. Liedmann and C. Wietfeld, "SoMoS—A multidimensional radio field based soil moisture sensing system," in *Proc. IEEE SENSORS*, Oct. 2017, pp. 1–3.

[12] X. Dong, M. C. Vuran, and S. Irmak, "Autonomous precision agriculture through integration of wireless underground sensor networks with center pivot irrigation systems," *Ad Hoc Netw.*, vol. 11, no. 7, pp. 1975–1987, 2013.

[13] M. J. Tiusanen, "Soil scouts: Description and performance of single hop wireless underground sensor nodes," *Ad Hoc Netw.*, vol. 11, no. 5, pp. 1610–1618, 2013.

[14] A. Salam and S. Shah, "Internet of Things in smart agriculture: Enabling technologies," in *Proc. IEEE 5th World Forum Internet Things (WF-IoT)*, Limerick, Ireland, Apr. 2019, pp. 692–695.

[15] M. Hardie and D. Hoyle, "Underground wireless data transmission using 433-MHz LoRa for agriculture," *Sensors*, vol. 19, no. 19, p. 4232, Sep. 2019.

[16] M. Gineprini, S. Parrino, G. Peruzzi, and A. Pozzebon, "LoRaWAN performances for underground to aboveground data transmission," in *Proc. IEEE Int. Instrum. Meas. Technol. Conf. (I2MTC)*, May 2020, pp. 1–6.

[17] A. Abrardo and A. Pozzebon, "A multi-hop LoRa linear sensor network for the monitoring of underground environments: The case of the medieval aqueducts in Siena, Italy," *Sensors*, vol. 19, no. 2, p. 402, Jan. 2019.

[18] L. Parri, S. Parrino, G. Peruzzi, and A. Pozzebon, "Low power wide area networks (LPWAN) at sea: Performance analysis of offshore data transmission by means of LoRaWAN connectivity for marine monitoring applications," *Sensors*, vol. 19, no. 14, p. 3239, Jul. 2019.

[19] A. R. Silva and M. Moghaddam, "Design and implementation of low-power and mid-range magnetic-induction-based wireless underground sensor networks," *IEEE Trans. Instrum. Meas.*, vol. 65, no. 4, pp. 821–835, Apr. 2016.

[20] E. H. A. Duisterwinkel, E. Talnishnikh, D. Krijnders, and H. J. Wortche, "Sensor motes for the exploration and monitoring of operational pipelines," *IEEE Trans. Instrum. Meas.*, vol. 67, no. 3, pp. 655–666, Mar. 2018.

[21] C. Ebi, F. Schaltegger, A. Rust, and F. Blumensaat, "Synchronous LoRa mesh network to monitor processes in underground infrastructure," *IEEE Access*, vol. 7, pp. 57663–57677, 2019.

[22] H.-C. Lee and K.-H. Ke, "Monitoring of large-area IoT sensors using a LoRa wireless mesh network system: Design and evaluation," *IEEE Trans. Instrum. Meas.*, vol. 67, no. 9, pp. 2177–2187, Sep. 2018.

[23] M. Cattani, C. Boano, and K. Römer, "An experimental evaluation of the reliability of LoRa long-range low-power wireless communication," *J. Sensor Actuat. Netw.*, vol. 6, no. 2, p. 7, Jun. 2017.

[24] X.-F. Wan, Y. Yang, X. Du, and M. S. Sardar, "Design of propagation testnode for LoRa based wireless underground sensor networks," in *Proc. Prog. Electromagn. Res. Symp.*, Nov. 2017, pp. 579–583.

[25] X.-F. Wan, Y. Yang, J. Cui, and M. S. Sardar, "Lora propagation testing in soil for wireless underground sensor networks," in *Proc. 6th Asia–Pacific Conf. Antennas Propag. (APCAP)*, Oct. 2017, pp. 1–3.

[26] W. Xue-fen, D. Xing-jing, Y. Yi, Z. Jing-wen, M. S. Sardar, and C. Jian, "Smartphone based LoRa in-soil propagation measurement for wireless underground sensor networks," in *Proc. IEEE Conf. Antenna Meas. Appl. (CAMA)*, Dec. 2017, pp. 114–117.

[27] A. Grunwald, M. Schaarschmidt, and C. Westerkamp, "LoRaWAN in a rural context: Use cases and opportunities for agricultural businesses," in *Proc. Mobile Commun.-Technol. Appl.*, May 2019, pp. 1–6.

[28] X. Yu, P. Wu, Z. Zhang, N. Wang, and W. Han, "Electromagnetic wave propagation in soil for wireless underground sensor networks," *Prog. Electromagn. Res. M*, vol. 30, pp. 11–23, 2013.

[29] L. Li, N. Dong, and J. Chen, "EM wave propagation in non-uniform soil," *Inf. Technol. J.*, vol. 12, no. 19, pp. 5011–5016, Sep. 2013.

[30] A. Salam and M. C. Vuran, "Impacts of soil type and moisture on the capacity of multi-carrier modulation in Internet of underground Things," in *Proc. 25th Int. Conf. Comput. Commun. Netw. (ICCCN)*, Aug. 2016, pp. 1–9.

[31] M. Dobson, F. Ulaby, M. Hallikainen, and M. El-rayes, "Microwave dielectric behavior of wet soil—Part II: Dielectric mixing models," *IEEE Trans. Geosci. Remote Sens.*, vols. GE–23, no. 1, pp. 35–46, Jan. 1985.

[32] A. Salam, M. C. Vuran, and S. Irmak, "Pulses in the sand: Impulse response analysis of wireless underground channel," in *Proc. 35th Annu. IEEE Int. Conf. Comput. Commun.*, Apr. 2016, pp. 1–9.

[33] A. Sadeghioon, D. Chapman, N. Metje, and C. Anthony, "A new approach to estimating the path loss in underground wireless sensor networks," *J. Sensor Actuat. Netw.*, vol. 6, no. 3, p. 18, Aug. 2017.

[34] X. Dong and M. C. Vuran, "Impacts of soil moisture on cognitive radio underground networks," in *Proc. 1st Int. Black Sea Conf. Commun. Netw. (BlackSeaCom)*, Jul. 2013, pp. 222–227.

[35] X. Yu, W. Han, and Z. Zhang, "Path loss estimation for wireless underground sensor network in agricultural application," *Agricult. Res.*, vol. 6, no. 1, pp. 97–102, Mar. 2017.

[36] M. C. Vuran and I. F. Akyildiz, "Channel model and analysis for wireless underground sensor networks in soil medium," *Phys. Commun.*, vol. 3, no. 4, pp. 245–254, Dec. 2010.

[37] Z. Sun, I. F. Akyildiz, and G. P. Hancke, "Dynamic connectivity in wireless underground sensor networks," *IEEE Trans. Wireless Commun.*, vol. 10, no. 12, pp. 4334–4344, Dec. 2011.

[38] D. W. Sambo, A. Forster, B. O. Yenke, and I. Sarr, "A new approach for path loss prediction in wireless underground sensor networks," in *Proc. IEEE 44th LCN Symp. Emerg. Topics Netw.*, Oct. 2019, pp. 50–57.

[39] V. L. Mironov, L. G. Kosolapova, and S. V. Fomin, "Physically and mineralogically based spectroscopic dielectric model for moist soils," *IEEE Trans. Geosci. Remote Sens.*, vol. 47, no. 7, pp. 2059–2070, Jul. 2009.

[40] (Aug. 2019). *International Telecommunication Union (ITU), Electrical Characteristics of the Surface of the Earth*. Accessed: Nov. 3, 2020. [Online]. Available: https://www.itu.int/dms_pubrec/itu-r/rec/p/R-REC-P.527-4-201706-I!!PDF-E.pdf

[41] STMicroelectronics. (Jun. 2018). *UM2115 User Manual*. Accessed: Jul. 9, 2020. [Online]. Available: https://www.st.com/content/ccc/resource/technical/document/user_manual/group0/ac/62/15/c7/60/ac/4e/9c/DM00329995/files/DM00329995.pdf/jcr:content/translations/en.DM00329995.pdf

[42] STMicroelectronics. (Sep. 2017). *STM32L072x8, STM32L072xB and STM32L072xZ Datasheet*. Accessed: Sep. 9, 2020. [Online]. Available: https://www.st.com/resource/en/datasheet/stm32l072cz.pdf

[43] Semtech. (Jan. 2019). *SX1276/77/78/79 Datasheet*. Accessed: Jul. 9, 2020. [Online]. Available: https://www.semtech.com/uploads/documents/DS_SX1276-7-8-9_W_APP_V6.pdf

[44] Dragino. (Jun. 2020). *LG308 LoRaWAN Gateway Datasheet V1.3.0*. Accessed: Jul. 20, 2020. [Online]. Available: https://www.dragino.com/downloads/downloads/LoRa_Gateway/LG308-LG301/LG308_LoRaWAN_Gateway_User_Manual_v1.3.0.pdf

[45] Semtech. (Mar. 2018). *SX1257 Low Power Digital I and Q RF Multi-PHY Mode Transceiver Datasheet*. Accessed: Jul. 9, 2020. [Online]. Available: https://www.semtech.com/uploads/documents/DS_SX1257_V1.2.pdf

[46] Semtech. (Jun. 2017). *SX1301 Datasheet*. Accessed: Jul. 9, 2020. [Online]. Available: https://www.semtech.com/uploads/documents/sx1301.pdf

[47] R. L. Folk and W. C. Ward, "Brazos River bar [Texas]; A study in the significance of grain size parameters," *J. Sedimentary Res.*, vol. 27, no. 1, pp. 3–26, Mar. 1957.

[48] C. K. Wentworth, "A scale of grade and class terms for clastic sediments," *J. Geol.*, vol. 30, no. 5, pp. 377–392, Jul. 1922.

[49] G. Sarti *et al.*, "Magdala harbour sedimentation (Sea of galilee, Israel), from natural to anthropogenic control," *Quaternary Int.*, vol. 303, pp. 120–131, Jul. 2013.

[50] K. Prakash, A. Sridharan, H. K. Thejas, and H. M. Swaroop, "A simplified approach of determining the specific gravity of soil solids," *Geotechnical Geol. Eng.*, vol. 30, no. 4, pp. 1063–1067, Aug. 2012.

[51] E. P. Stuntebeck, D. Pompili, and T. Melodia, "Wireless underground sensor networks using commodity terrestrial motes," in *Proc. 2nd IEEE Workshop Wireless Mesh Netw.*, Reston, VA, USA, Sep. 2006, pp. 112–114.

[52] B. Van Hieu, S. Choi, Y. U. Kim, Y. Park, and T. Jeong, "Wireless transmission of acoustic emission signals for real-time monitoring of leakage in underground pipes," *KSCE J. Civil Eng.*, vol. 15, no. 5, pp. 805–812, May 2011.
[53] B. Silva, R. M. Fisher, A. Kumar, and G. P. Hancke, "Experimental link quality characterization of wireless sensor networks for underground monitoring," *IEEE Trans. Ind. Informat.*, vol. 11, no. 5, pp. 1099–1110, Oct. 2015.
[54] I. Zaman, J. Dede, M. Gellhaar, H. Koehler, and A. Foerster, "Molenet: A new sensor node for underground monitoring," in *Proc. IEEE 41st Conf. Local Comput. Netw. Workshops (LCN Workshops)*, Dubai, United Arab Emirates, Nov. 2016, pp. 145–147.
[55] R. Cardell-Oliver, C. Hübner, M. Leopold, and J. Beringer, "Dataset: LoRa underground farm sensor network," in *Proc. 2nd Workshop Data Acquisition Anal.*, New York, NY, USA, Nov. 2019, pp. 26–28.
[56] A. J. Wixted, P. Kinnaird, A. Tait, A. Ahmadinia, and N. Strachan, "Evaluation of LoRa and LoRaWAN for wireless sensor networks," in *Proc. IEEE Sensors*, Orlando, FL, USA, Oct. 2016, pp. 1–3.
[57] J. Petäjäjärvi, K. Mikhaylov, M. Pettissalo, J. Janhunen, and J. Iinatti, "Performance of a low-power wide-area network based on LoRa technology: Doppler robustness, scalability, and coverage," *Int. J. Distrib. Sensor Netw.*, vol. 13, no. 3, Mar. 2017, Art. no. 155014771769941.
[58] P. J. Radcliffe, K. G. Chavez, P. Beckett, J. Spangaro, and C. Jakob, "Usability of LoRaWAN technology in a central business district," in *Proc. IEEE 85th Veh. Technol. Conf. (VTC Spring)*, Sydney, NSW, Australia, Jun. 2017, pp. 1–5.
[59] *MathWorks Earth Surface Permittivity MATLAB Function*. Accessed: Nov. 4, 2020. [Online]. Available: https://www.mathworks.com/help/comm/ref/earthsurfacepermittivity.html

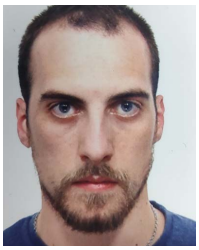

Gabriele Di Renzone received the M.Sc. degree in electronics and communications engineering from the University of Siena, Siena, Italy, in 2020, where he is currently pursuing the Ph.D. degree.

His research topic focuses on the study of subgigahertz, low-power wide-area networks (LPWANs) applied in the Industrial Internet of Things (IIoT) scenario, where the presence of metal objects compromises the transmission capabilities. Therefore, he aims to design and characterize low-power devices that rely on subgigahertz, wireless sensor networks (WSNs) for tracking and monitoring purposes.

Stefano Parrino received the M.Sc. degree in telecommunications engineering with a focus on radio frequency identification (RFID) technology applied to healthcare environments from the University of Siena, Siena, Italy, in 2008.

He is currently a Research Fellow at the Department of Information Engineering and Mathematics, University of Siena. His main research activities focus on RFID applications and design and development of embedded monitoring systems based on low-power wide-area networks (LPWANs), microcontrollers, and wireless sensor networks (WSNs) applied in different application fields.

Giacomo Peruzzi received the B.Sc. degree in information engineering and the M.Sc. degree in computer and automation engineering from the University of Siena, Siena, Italy, in 2016 and 2019, respectively, where he is currently pursuing the Ph.D. degree in information engineering with the Department of Information Engineering and Mathematics.

His research activity principally falls within the fields of the Internet of Things (IoT) and Industry 4.0. In particular, he deals with wireless sensor networks (WSNs) for monitoring systems that are enabled by low-power wide-area network (LPWAN) technologies.

Alessandro Pozzebon (Member, IEEE) received the M.Sc. degree in information engineering with a focus on the radio frequency identification (RFID) technology applied to cultural heritage and the Ph.D. degree from the University of Siena, Siena, Italy, in 2006 and 2012, respectively. His Ph.D. thesis was on the use of RFID technology for environmental monitoring of coastal erosion phenomena.

He is currently an Assistant Professor with the Department of Information Engineering and Mathematics, University of Siena, where he teaches in the Laboratory of Internet of Things. His main research interests include the development of applications based on low-power wide-area network (LPWAN), wireless sensor networks (WSNs), and RFID technologies in several different application fields from healthcare to cultural heritage and environmental monitoring.

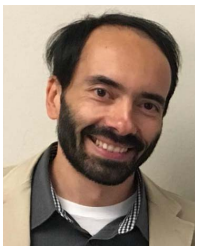

Duccio Bertoni received the M.Sc. and Ph.D. degrees from the Department of Earth Sciences, University of Pisa, Pisa, Italy, in 2005 and 2010, respectively. His Ph.D. thesis dealt with the morphodynamic evolution of three artificial pebble beaches at Marina di Pisa, Italy.

He held several post-doctoral positions at the University of Pisa from 2010 to 2012 and at the Department of Physics and Earth Sciences, University of Ferrara, Ferrara, Italy, from 2013 to 2015. Since 2017, he has been an Assistant Professor at the Department of Earth Sciences, University of Pisa, where he is a Lecturer in coastal sediment dynamics.